Artificial Intelligence In Medicine 154 (2024) 102918

Contents lists available at ScienceDirect

Artificial Intelligence In Medicine

journal homepage: www.elsevier.com/locate/artmed

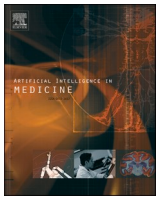

Research paper

A new methodology for determining the central pressure waveform from peripheral measurement using Fourier-based machine learning

Arian Aghilinejad *, Alessio Tamborini, Morteza Gharib

Division of Engineering and Applied Science, California Institute of Technology, Pasadena, CA, United States

ARTICLE INFO

Keywords:
Blood pressure
Hemodynamics
Machine learning
Wearable electronics
Transfer function
Central pressure

ABSTRACT

Radial applanation tonometry is a well-established technique for hemodynamic monitoring and is becoming popular in affordable non-invasive wearable healthcare electronics. To assess the central aortic pressure using radial-based measurements, there is an essential need to develop mathematical approaches to estimate the central pressure waveform. In this study, we propose a new Fourier-based machine learning (F-ML) methodology to transfer non-invasive radial pressure measurements to the central pressure waveform. To test the method, collection of tonometry recordings of the radial and carotid pressure measurements are used from the Framingham Heart Study (2640 individuals, 55 % women) with mean (range) age of 66 (40–91) years. Method-derived estimates are significantly correlated with the measured ones for three major features of the pressure waveform (systolic blood pressure, r=0.97, $p < 0.001$; diastolic blood pressure, r=0.99, $p < 0.001$; and mean blood pressure, r=0.99, $p < 0.001$). In all cases, the Bland-Altman analysis shows negligible bias in the estimations and error is bounded to 5.4 mmHg. Findings also suggest that the F-ML approach reconstructs the shape of the central pressure waveform accurately with the average normalized root mean square error of 5.5 % in the testing population which is blinded to all stages of machine learning development. The results show that the F-ML transfer function outperforms the conventional generalized transfer function, particularly in terms of reconstructing the shape of the central pressure waveform morphology. The proposed F-ML transfer function can provide accurate estimates for the central pressure waveform, and ultimately expand the usage of non-invasive devices for central hemodynamic assessment.

1. Introduction

The arterial pressure waveform and its morphological characteristics have been widely recognized as valuable sources of information for evaluating the cardiovascular state [1–8]. In recent years, a variety of new medical technologies have been developed to assess cardiac function and health using the peripheral pressure measurement [9–14]. In particular, the radial pressure waveform is generally preferred due to its lower variability between examiners, as well as its greater comfort for patients [15,16]. Moreover, measuring the radial pressure pulse is of great interest due to its accessibility in wrist-worn wearable devices [16]. In order to assess the central pressure and hemodynamics using such peripheral-based measurements, there is an essential need of transferring the peripheral measurement to the central estimation. The generalized transfer function (GTF) [17] is the most widely adopted transfer function among the existing methods to estimate the central pressure waveform from the peripheral measurement. To obtain the GTF, multiple individual transfer functions are averaged. This procedure introduces inaccuracy due to the non-negligible variability in the physiological parameters between subjects [18,19]. Additionally, previous studies reported poor generalizability for this method when applied to a new group of subjects based on the priorly generated GTF [19,20].

To overcome the shortcoming and weakness of the GTF, several adaptive methods have been proposed based on patient-specific physiological characteristics. For example, Stergiopulos et al. [21] developed a time-domain approach where the forward and backward components of the blood pressure signal are separated to obtain a rigorous model for transferring the pressure waveform. In another study, Zhang et al. [20] proposed the multi-channel blind system identification algorithm to estimate the central pressure waveform. The main advantage of this approach is that it only requires knowledge from the output (central) signal [18,19]. In addition, there have been other alternative methods developed based on parallel tube models, model-based system

* Corresponding author.
E-mail address: aghili@caltech.edu (A. Aghilinejad).

https://doi.org/10.1016/j.artmed.2024.102918
Received 25 September 2023; Received in revised form 2 April 2024; Accepted 17 June 2024
Available online 18 June 2024

identification and lumped parameter modeling for estimating the central pressure waveform [22–24]. However, some of these methods rely on brute-force optimization of parameters which are not necessarily physiological. In addition, these methods mostly require multiple peripheral measurements which limits their practical clinical usefulness [18,19].

Recent advances in artificial intelligence and machine learning (ML) bring new research possibilities and approaches in cardiovascular engineering [25–29]. As examples, Jin et al. [30] showed possibility of assessing vascular ageing based on a single peripheral pulse wave to estimate carotid-femoral pulse wave velocity using ML models. Aghilinejad et al. [31] showed the applicability of regression analysis in estimating wave intensity based on single pressure waveform measurement. In addition, there has been emerging interest in employing ML-based approaches for better estimating the central pressure waveform from peripheral measurements. Liu et al. [19] introduced a temporal convolutional network to reconstruct the central pressure waveform from radial blood pressure. Du et al. [32] proposed a two-level adaptive transfer function strategy to estimate high-frequency components of the aortic pressure waveform from brachial measurements. Their findings suggest that the proposed two-level adaptive transfer function improves capturing the shape and high-frequency components of aortic pressure waveform compared with GTF as a reference baseline method. Magbool et al. [18] developed a hybrid approach based on machine-learning models with cross relation blind estimation approach to estimate aortic blood pressure from peripheral measurements and tested their approach on a virtual database. However, due to the absence of large heterogeneous clinical datasets, the potential clinical application of such methods has not been tested.

In this study, we propose and evaluate a new Fourier-based ML (F-ML) transfer function to reconstruct the central pressure waveform from a peripheral radial measurement. We used the large heterogeneous population of the Framingham Offspring Cohort [33,34] to conduct a rigorous analysis on the accuracy of the proposed F-ML transfer function. In contrast to most research in the field of cardiovascular engineering utilizing synthetic datasets [18], utilizing the heterogenous clinical dataset in this study can practically assess the applicability of our method. We also tested the generalizability of this approach in different regression models. The ability of the proposed method is not only examined in capturing the major features of the central pressure waveform (e.g., systolic blood pressure), its performance is also evaluated in reconstructing the shape of the central pressure waveform.

2. Materials and methods

2.1. Participants and data

In this study, we utilize a subset of data from the Framingham Heart Study (FHS), a population-based epidemiological cohort analysis. The subset consists of participants from the Offspring cohort, which has been previously described [33,35]. The cohort comprises a diverse group of $N = 2640$ participants, including 1201 males and 1439 females, with an age range from 40 to 91 years old. This population includes 395 individuals with cardiovascular disease (defined by Framingham investigators [34] and including myocardial infarction, coronary insufficiency, stroke, heart failure, or cardiovascular-related death). Table 1 summarizes the characteristics of the total participants as well as two generated datasets for training and testing purposed (70/30 split). These individuals underwent thorough non-invasive evaluations of central hemodynamics, resulting in a comprehensive collection of tonometry recordings for carotid and radial pressure waveforms [34]. The calibration procedure is performed as in previous studies [33,34,36]. Participants were studied in the supine position after resting for around 5 min. Supine brachial systolic and diastolic blood pressures were obtained with the use of an oscillometric device and were assigned to the peak and minima of the brachial pulse waveform, respectively.

Table 1
Baseline characteristics of total patient data ($N = 2640$), the training subpopulation ($N = 1848$), and the testing subpopulation ($N = 792$).

Variable	Total (N = 2640)	Training (N = 1848)	Test (N = 792)
Age, y	66 ± 9	66 ± 9	66 ± 9
Women, N (%)	1439 (55)	1000 (54)	439 (55)
Height, cm	167 ± 10	167 ± 10	167 ± 9
Weight, kg	79 ± 17	79 ± 18	78 17
Body mass index, kg/m^2	27.9 ± 5.1	27.9 ± 5.1	27.9 ± 5.1
Heart rate, bpm	62 ± 10	62 ± 10	62 ± 10
Brachial blood pressure, mmHg			
Systolic	140 ± 20	140 ± 20	140 ± 20
Diastolic	69 ± 9	69 ± 9	69 ± 9
Pulse	71 ± 19	71 ± 19	71 ± 19
Subject with cardiovascular disease, N (%)	395 (15)	274 (15)	121 (15)

All values are (mean ± SD) except as noted.

The mean brachial artery pressure was calculated from numeric integral of the calibrated brachial pressure pulse. With assignment of the same mean and diastolic pressures to the carotid and radial pulse recording, both these pressure waves were calibrated throughout the cardiac cycle. Tonometry data was digitized during the primary acquisition at the rate of 1000 Hz. Waveforms were then signal-averaged using the ECG R-wave as a fiducial point. Calibrated carotid pressure is used as a surrogate for central pressure [36,37]. All participants provided written informed consent, and the protocols were approved by the Boston University Medical Campus and Boston Medical Center Institutional Review Board.

2.2. Fourier representation of the pressure waveform

To transform data from this high-dimensional input signal space to a low-dimensional one, we utilized Fourier-based decomposition. The Fourier series represents a synthesis of a periodic function by summing harmonically related sinusoids and cosinusoides. An arbitrary periodic pressure function $P(t)$ can be represented as a Fourier series with N oscillatory components. A common form of the Fourier series decomposition is defined as:

$$P(t) = \frac{a_0}{2} + \sum_{n=1}^{N} \left(a_n cos\left(\frac{2\pi}{T} nt\right) + b_n sin\left(\frac{2\pi}{T} nt\right) \right), \quad (1)$$

where T is the period of the pressure function $P(t)$ (i.e., the cardiac cycle or inverse of heart rate (HR) for blood pressure waveform). In conducting the Fourier decomposition here, we used the sinusoid-cosinusoide form to extract the coefficients at different frequencies for constructing input features for machine learning. Coefficients a_n and b_n are associated with each individual harmonic (cosine and sine) corresponding to different frequencies $f_n = \frac{n}{T}$, and can be calculated by the Fourier transform given by:

$$a_n = \frac{2}{T} \int_0^T P(t) cos\left(\frac{2\pi}{T} nt\right) dt, \quad (2)$$

$$b_n = \frac{2}{T} \int_0^T P(t) sin\left(\frac{2\pi}{T} nt\right) dt, n \epsilon (0, \infty). \quad (3)$$

By obtaining the coefficients using Eqs. (2) and (3), we represent the pressure waveform $\widetilde{P}(t)$ with finite selected frequency (i.e., $n = 0$ to N) by adding up individual harmonic component (Eq. (1)). In this study, the features of the pressure wave were extracted as the first N^{th} low frequency components of the waveforms using the Fast Fourier Transform (FFT). Fig. S1 in the Supplementary material represents the associated error between the measured and reconstructed pressure waveform based on the limited number of Fourier coefficients. As it can be noticed from this figure, the error between the measured pressure and the

reconstructed one is marginal after $N = 20$. The selected input features in this study (depending on the chosen number of Fourier modes; *FN*) consists of *FN* cosine coefficients and (*FN* - 1) sine coefficients (sine b_0 is always equal to zero).

2.3. Regression models and Fourier-based machine learning transfer function

We employ three regression models to evaluate the accuracy of the F-ML transfer function. These models include the Lasso regressor, support vector regressor, and gradient boosted decision-tree, which are among the well-established models extensively used in previous works [28,31,38]. Each of these models is trained on features derived from the Fourier decomposition of the pressure waveform, as shown in Fig. 1. Initially, the clinical dataset is split into training and testing data for all machine learning analyses. The models are strictly trained on the training population based on the Fourier decomposition of the radial and central pressure waveforms. The models are trained with the Fourier modes of the radial waveforms as input and the Fourier modes of the central waveforms as output. As in Fig. 1 shown, the input of the machine learning model consists of a vector of sine and cosine numeric coefficients derive from Fourier decomposition of the radial pressure waveform, and the output of the machine learning model is the vector of sine and cosine numeric coefficients needed for central pressure construction. After training, the testing dataset is used only once to evaluate the accuracy of the model. The radial waveform in the testing dataset is first decomposed into Fourier modes and given to the predictive model. The output of the predictive models, which use the estimated modes of the corresponding central waveform, is then inverse Fourier transformed to the time domain using the computed modes as well as the length of the signal. The combination of the predictive model and the inverse Fourier transform is called the F-ML Transfer Function (Fig. 1). Lastly, the computed transferred central waveform is compared with the measured central waveform, and the relevant metrics are reported in this study (see the statistical analysis section).

Fig. S2 presents the correlation matrix, reporting the inter-feature correlations for five Fourier modes (FN = 5; input size = 9). Python's sklearn and TensorFlow packages are used for data pre-processing (e.g., normalization), training, and testing the algorithms. The training and testing data split is 70 % and 30 %, respectively. The pandas and numpy packages are also used for data processing. The three methods of machine learning (Lasso regressor, support vector regressor, and gradient boosted decision-tree) are chosen to examine the applicability of our approach and is based on the popularity of these methods in previous

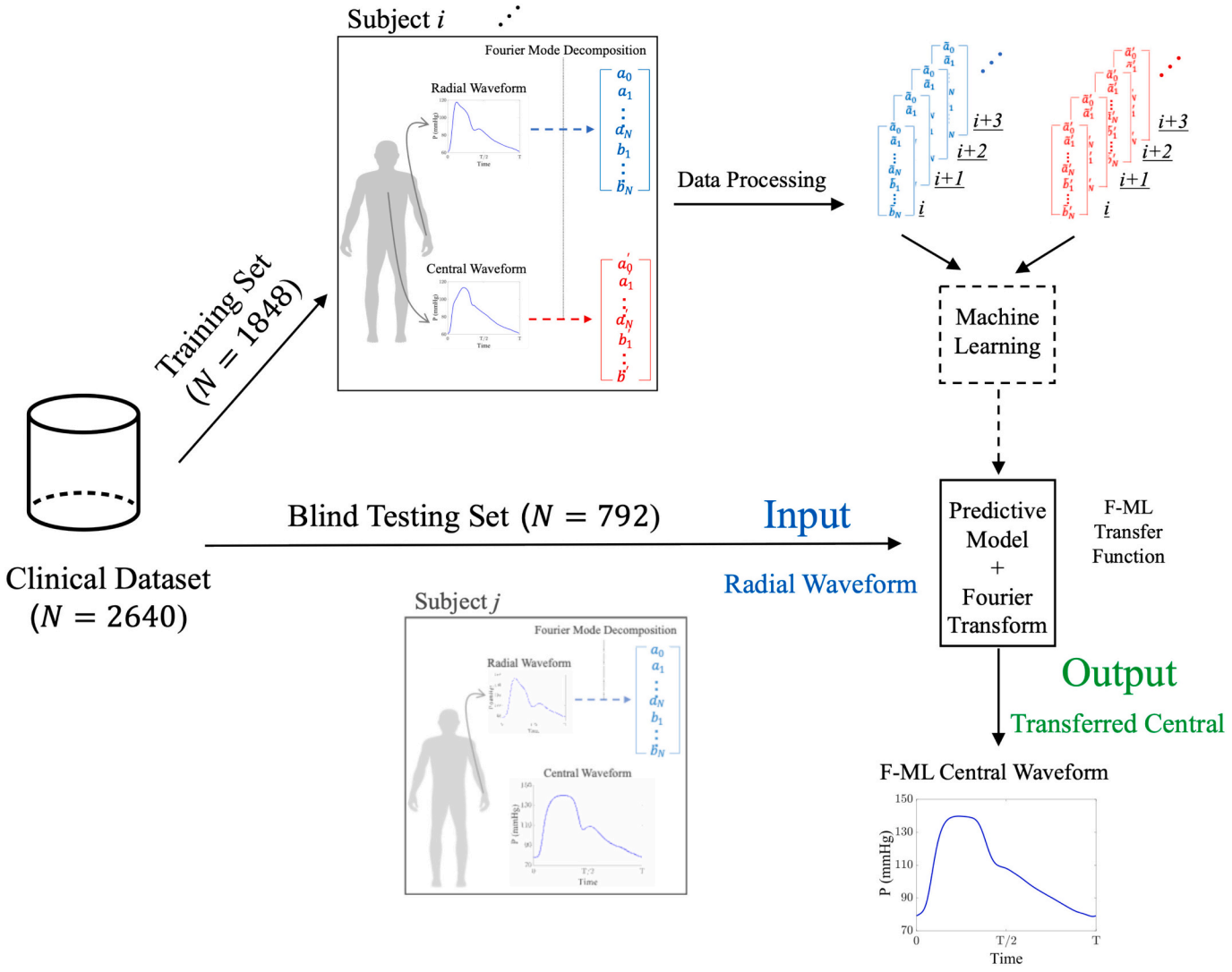

Fig. 1. Schematic of the Fourier-based machine learning (F-ML) transfer function for computing the central pressure waveform. Initially, the clinical dataset is split into training and testing data for all machine learning analyses. The models are strictly trained on the training population based on the Fourier decomposition of the radial and central pressure waveforms. The accuracy of the approach is measured using the testing dataset which is used only once.

cardiovascular engineering studies [30,31,38]. Lasso regression, or Least Absolute Shrinkage and Selection Operator, is a linear regression technique chosen for its simplicity and regularization properties to mitigate overfitting. Support vector regressor, akin to Support Vector Machines in classification, aims to identify the hyperplane that best fits the data points within a specified margin of tolerance. Finally, gradient boosted decision-tree represents an ensemble learning approach that amalgamates decision trees with gradient boosting. This method incrementally adds decision trees to an ensemble, with each subsequent tree rectifying errors made by its predecessors. The hyperparameters in the models are found using a ten-fold cross-validation (CV) scheme using the GridSearchCV library. The comprehensive list of examined hyperparameters for different ML models is demonstrated in Table S1. Hyperparameters not reported in Table S1 are set to their default values. For all models, the combination of hyperparameters attributed to the highest accuracy for training is chosen. The hyperparameter values selected for the final models were highlighted by underlining and bold font in Table S1.

2.4. Generalized transfer function (GTF)

To provide a reference for the accuracy of the proposed method, we also implement a GTF [17]. Given the Fourier representations $\widetilde{P}_{\mathrm{rad}}(\omega)$ and $\widetilde{P}_{\mathrm{cen}}(\omega)$ of the radial and central pressure waveforms (calculated via a Fast Fourier Transform of the time-signals), the radial-based transfer function is defined as for angular frequency ω and phase $\varphi_{\mathrm{rad}}(\omega)$ (resp. $\varphi_{\mathrm{cen}}(\omega)$) of the radial (resp. central) pressure waveforms. Here, $|\bullet|$ denotes the complex magnitude of the respective Fourier component. Phases are adjusted by adding or subtracting integral values of 2π such that all angles consistently fell within $(-\pi, \pi]$. The corresponding GTF is obtained by averaging all such individual transfer functions (computed from each pair of radial and central pressure waveform patient data) over bins of length 1 Hz. Use of this transfer function for radial-based measurements has been well-established and validated clinically [17,39–42],

$$H_{\mathrm{cen-rad}}(\omega) = \frac{|\widetilde{P}_{\mathrm{rad}}(\omega)|}{|\widetilde{P}_{\mathrm{cen}}(\omega)|} e^{i\varphi_{\mathrm{rad-cen}}}. \tag{4}$$

2.5. Statistical analysis

Baseline characteristics for the study sample are demonstrated in Table 1, and continuous variables derived from the sample data are summarized as mean ± standard deviation (SD). To assess the accuracy of the proposed F-ML transfer function, we evaluated Pearson correlation coefficients r, coefficient of determination R^2, and root mean square errors (RMSE) of three major features of the pressure waveform: systolic, diastolic and mean pressure during one cardiac cycle. Statistical significance is defined as $p<0.001$. We also report the normalized RMSE (nRMSE) which is computed based on the range of the dependent variable (difference between the maximum and the minimum). In addition to quantifying the error associated with reconstructing the pressure waveform, we also computed the nRMSE associated with reconstructing the first and second derivative of the pressure waveform. The derivatives are calculated using discrete differentiation and Savitsky-Golay filters. The agreement and bias between the transferred and measured variables are evaluated by Bland-Altman analysis presented as mean differences with limits of agreement (mean bias ±1.96 SD of the differences). Levene's test for homogeneity of variance is conducted for error distributions. Kruskal-Wallis' rank-sum test with Bonferroni adjustment is employed for comparing the error distributions of F-ML and GTF. All statistical analysis on the clinical data is performed using custom written codes implemented in Matlab (R2020b, The Mathworks Inc.).

3. Results

3.1. Accuracy of the F-ML transfer function

Table 2 presents the correlation, coefficient of determination, errors, and agreement for three features of the central pressure waveform (i.e., systolic blood pressure (SBP), diastolic blood pressure (DBP), and mean blood pressure (MBP)) that are evaluated from the measured central waveform and the estimated one from the transferred central waveform using F-ML transfer function. The analysis is conducted for three different regression models to evaluate the applicability of the F-ML for transferring the pressure waveform. In this analysis, we utilized the first 20 Fourier modes of the pressure waves, which guarantees capture all features of the pressure waveform (see Fig. S1). In all three models, three major features of the central pressure waveform are well-correlated with strong coefficient of determination. As demonstrated by the mean difference from the Bland-Altman analysis that is reported in Table 2, the systemic bias between the measured values and F-ML transferred ones is negligible. In the last column of this table, the three features of the pressure waveform are also evaluated based on the transferred central waveform via GTF.

Fig. 2 demonstrates the Bland-Altman plots indicating the agreement between all intra-individual differences in the three major features of the central pressure waveform (SBP, DBP, and MBP) as well as the corresponding scatter plots between the measured and the method-derived transferred features. These results are reported for the support vector regressor model.

3.2. F-ML versus generalized transfer function

Fig. 3 demonstrates the distribution of the error between the transferred and measured central pressure waveform obtained via F-ML and GTF. Leven's test suggest that for the systolic and diastolic pressure, the variances for two groups are different ($p<0.001$), while for the mean pressure the test suggests that the variances are not significantly different ($p=0.662$). p-values from the Kruskal-Wallis' test for comparison of the two transferred methods are also reported in this figure. For the comparisons in this section, we used the support vector regressor

Table 2
Regression statistics between measured and transferred central pressure features in the blind test group ($N = 792$).

Machine learning model	Lasso	SVR	GBDT	GTF
Systolic blood pressure (SBP)				
Correlation coefficient (r)	0.97	0.97	0.96	0.94
Coefficient of determination (R^2)	0.93	0.94	0.91	0.87
RMSE (mmHg)	5.4	5.4	6.3	7.4
Limit of agreement (mmHg)	20.9	20.9	24.1	28.9
Mean difference (mmHg)	−1.0	−0.9	−1.2	0.8
Diastolic blood pressure (DBP)				
Correlation coefficient (r)	0.99	0.99	0.95	0.99
Coefficient of determination (R^2)	0.99	0.99	0.88	0.97
RMSE (mmHg)	1.0	1.3	2.8	1.5
Limit of agreement (mmHg)	3.9	5.1	10.9	2.6
Mean difference (mmHg)	0.3	0.2	0.4	1.4
Mean blood pressure (MBP)				
Correlation coefficient (r)	0.99	0.99	0.98	0.99
Coefficient of determination (R^2)	0.99	0.98	0.96	0.99
RMSE (mmHg)	0.9	0.8	2.6	0.9
Limit of agreement (mmHg)	3.4	3.4	8.8	3.4
Mean difference (mmHg)	0.0	0.0	−0.1	−0.1

Correlation coefficients have p-values<0.001 unless otherwise indicated. SVR and GTF stand for support vector regressor and generalized transfer function. GBDT stands for gradient boosted decision tree.

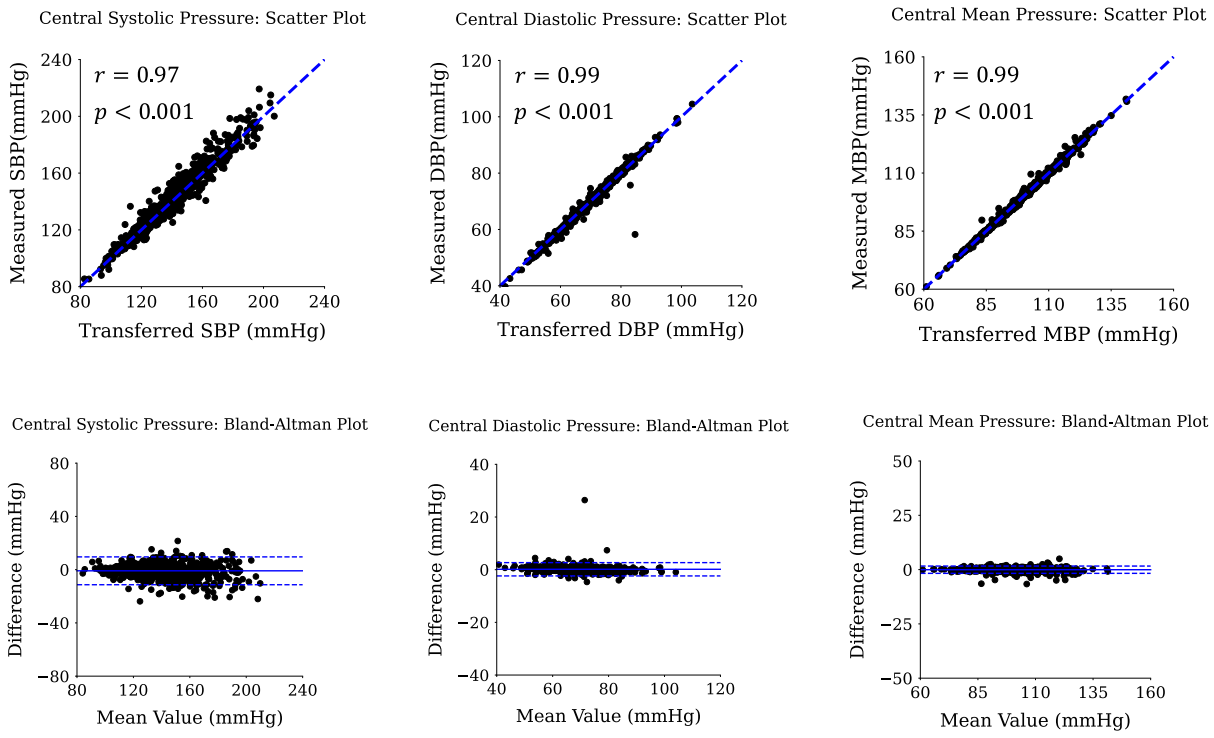

Fig. 2. Scatter and Bland-Altman plots for the central systolic, diastolic, and mean blood pressure amplitudes. The plots are demonstrated for the test data (N=792). Correlation (top row) and Agreement (bottom row) of peak amplitude values between measured values and those estimated by the Fourier-based machine learning transfer function based on the support vector regressor model.

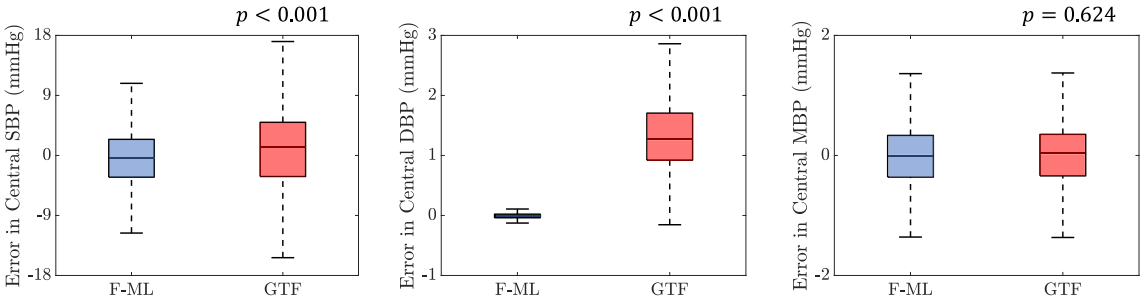

Fig. 3. Statistical analysis of the associated error between the transferred and measured central systolic, diastolic and mean pressure amplitudes. SBP indicates systolic blood pressure, DBP represents the diastolic blood pressure, and MBP represents the mean blood pressure. The blue boxplots (left) present the results for the Fourier-based Machine Learning (F-ML) transfer function and the red boxplots (right) present the results for the generalized transfer function (GTF). F-ML results are based on the support vector regressor. (For interpretation of the references to color in this figure legend, the reader is referred to the web version of this article.)

model. Note that both input and output waveforms have been calibrated using the same DBP and MBP values, therefore the GTF underperforms predicting DBP values while showing similar performance in predicting MBP.

Fig. 4 demonstrate six sample cases from the blind testing set that were transferred via proposed F-ML transfer function as well as the GTF. The measured central waveform is also overlaid with the dashed line for each case in this figure. Notably, test case 2 corresponds to an individual with cardiovascular disease, while the rest of the cases are for non-cardiovascular disease subjects. The first and second derivative of the transferred pressure waveform along with their corresponding measured one for test case 1 is presented in Fig. 5. Similar plots for the first and second pressure derivative comparison for other cases can be also found in the Supplementary material (Figs. S3 to S7).

Table 3 presents the associated error in the blind testing set between the transferred and measured central pressure waveform, once transferred via proposed F-ML transfer function, and once with the GTF. The comparison is conducted for the pressure waveform, the first derivative of the pressure waveform, and the second derivative of the pressure waveform. Fig. 6 provides the RMSE distribution for the similar comparison between the F-ML and GTF. Levene's test suggests that for all three error distributions, the variances for each group are different. p-Values from the Kruskal-Wallis' test for comparison of the two transferred methods for their RMSE distributions are also reported in this figure.

3.3. *Effect of the input Fourier modes in reconstructing the waveform*

Table 4 presents the nRMSE between the transferred pressure waveform and the measured pressure waveform, averaged in the blind testing set ($N = 792$) as a function of different number of Fourier modes to represent the input pressure waveform. In addition to the pressure waveform, this table also presents the average nRMSE in the blind testing set for the first and second derivative of the method-derived transferred and measured pressure waveform. NRMSE represents the point-by-point difference between each pair of pressure waveforms

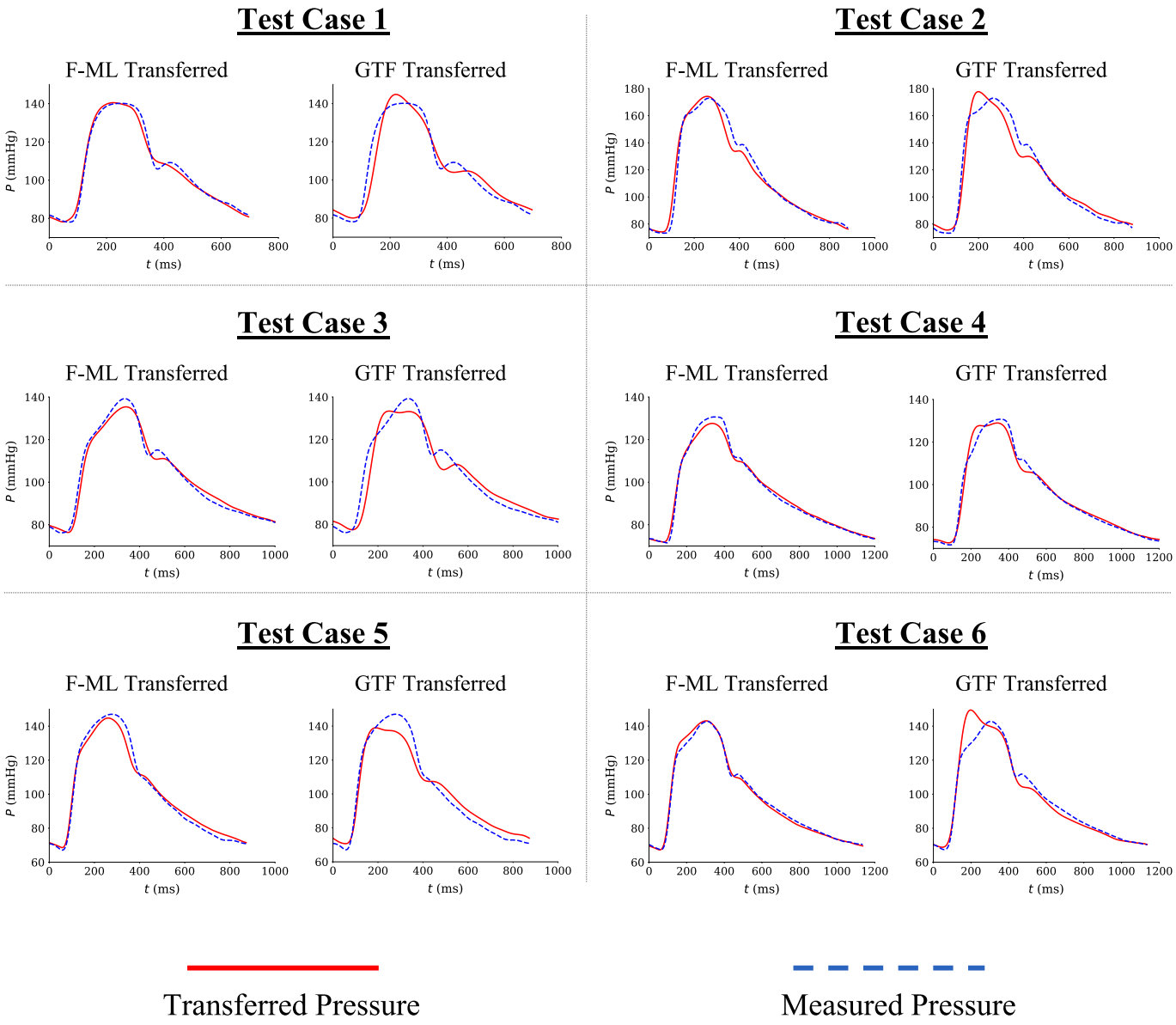

Fig. 4. Typical sample cases of the transferred and measured central pressure waveform. The left-hand-side figure in each panel presents the transferred waveform via Fourier-based machine learning (F-ML) transfer function, and the right-hand-side figure in each panel presents the transferred waveform via generalized transfer function (GTF). F-ML results are based on the support vector regressor.

(transferred and central) and hence, it is a strong metric to evaluate the accuracy of the transfer function in reconstructing the shape of the central pressure waveform. As it can be noticed from this table, after 10 input Fourier modes, the improvement in accuracy of the F-ML transfer function is not significant. The trend is consistent between all regression models. For reference, the nRMSE between the transferred pressure waveform using the GTF and the measured pressure waveform, averaged in the blind testing set ($N = 792$), is 7.8 %, 9.3 %, and 19.4 % for the pressure waveform, first derivative of the pressure waveform and second derivative of the pressure waveform, respectively.

3.4. Effect of the training size on method generalizability

Fig. 7 presents the averaged nRMSE over the blind testing set between the transferred pressure waveform and the measured one as a function of the training size. Similar figure can be found for the first derivative and the second derivative of the pressure waveform in the Supplementary material (Figs. S8 and S9). As it can be observed from these figures, including more data instances to the training sample after reaching 30 % of the entire dataset (corresponding to 792 instances) only marginally affects the accuracy of the method-derived transferred waveform.

4. Discussion

In this study, we introduced a new transfer function for determining central pressure waveform based on the radial measurement using F-ML approach. The method is tested in an extensive general cohort of the Framingham heart database and showed strong correlations for three major features of the pressure waveform including the central systolic pressure, central diastolic pressure, and central mean pressure. Findings suggest that our approach is able to reconstruct the shape of the central pressure waveform and its derivatives accurately. In addition, our results suggest that this new methodology outperforms the GTF in terms of reconstructing the central pressure waveform morphology as well as capturing the features of the central pressure waveform. Our results also suggest that the Fourier-based representation of the pressure wave can be tuned to reduce the input feature size without the major influence on

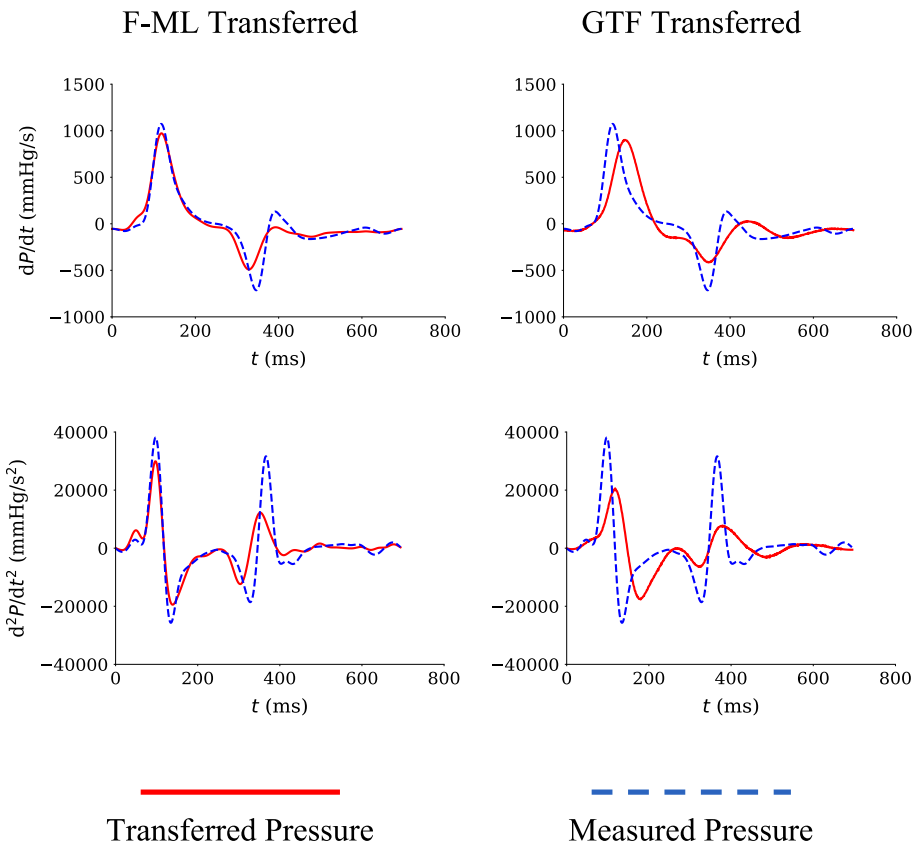

Fig. 5. Typical sample case of the transferred and measured first and second derivatives of the central pressure waveform. This sample case corresponds to the test case 1 in Fig. 4. The left-had-side figures present the transferred waveform via Fourier-based machine learning (F-ML) transfer function, and the right-hand-side figures present the transferred waveform via generalized transfer function (GTF). F-ML results are based on the support vector regressor.

Table 3
Comparison between the proposed F-ML and the GTF in the blind test group (N = 792).

Transfer function	Mean nRMSE of pressure waveform (%)	Mean nRMSE of the first derivative of the pressure waveform (%)	Mean nRMSE of the second derivative of the pressure waveform (%)
F-ML	5.5	5.9	9.0
GTF	7.8	9.3	19.4

nRMSE indicate the normalized root mean square error. F-ML and GTF stand for Fourier-based machine learning and generalized transfer function. F-ML model is based on support vector regressor with 20 input Fourier modes.

the accuracy of the model.

A first major finding of our study is that transferred central pressure waveforms based on the proposed F-ML approach significantly outperforms transfer based on the GTF, both in terms of capturing the features of the pressure waveform as well as reconstructing the shape of the pressure waveform. Table 2 and Fig. 2 suggest that three major features of the central pressure waveform, including the SBP, DBP and MBP, are strongly correlated with the measured ones. The maximum error associated for the three features is 6.3 mmHg corresponding to the systolic blood pressure for the gradient boosted decision tree model, which is still better than the error associated with the GTF (7.4 mmHg). Note that a high correlation and low margin for the error is reported in the blind testing set (never-seen-before-data by the model), which demonstrates the generalizability and true applicability of the method. High agreement can be also observed from the sample Bland-Altman plots demonstrated for three major features of the central pressure waveform in Fig. 2. In addition, the strong association found among different machine learning models demonstrates that Fourier decomposition provides sufficient information for training different regression models for the purpose of transferring peripheral measurements to the central estimation. However, there is marginal variability between different models in term of the accuracy (Table 2). Fig. 3 shows the distributions of the error between transferred features of the central pressure waveform and the measured ones for the proposed F-ML method as well as the GTF. These results show that the associated error for estimating the central systolic and diastolic blood pressure using the proposed method is much less than the similar error obtained using GTF (with significant statistical difference). The difference however is not significant for the mean blood pressure. The accuracy in estimating central mean and diastolic blood pressure is partially attributed to two factors: the calibration of the waveforms and the training-oriented approach of the proposed F-ML model. Both the F-ML model and the GTF utilized the same calibrated waveforms. Waveform calibration fixes DBP and MBP values, as a result we expect any transfer function that faithfully recovers waveform shape to capture these values very well. However, the GTF employs an averaging technique of individual transfer functions at specific fixed frequency bins to convert radial pressure to central pressure. This averaging effectively captures the low-frequency components crucial for defining mean blood pressure as presented in Fig. 3, ensuring that both F-ML and GTF perform similarly in estimating the mean. However, this averaging method leads to the loss of some crucial data necessary for accurately capturing extreme values such as systolic blood pressure. Capturing high-frequency component is essentially the advantage of the proposed F-ML. Overall, these findings suggest that the F-ML transfer function outperforms the commonly used GTF in terms of estimating the three major features of the central pressure waveform.

Another significant advantage of the proposed F-ML transfer

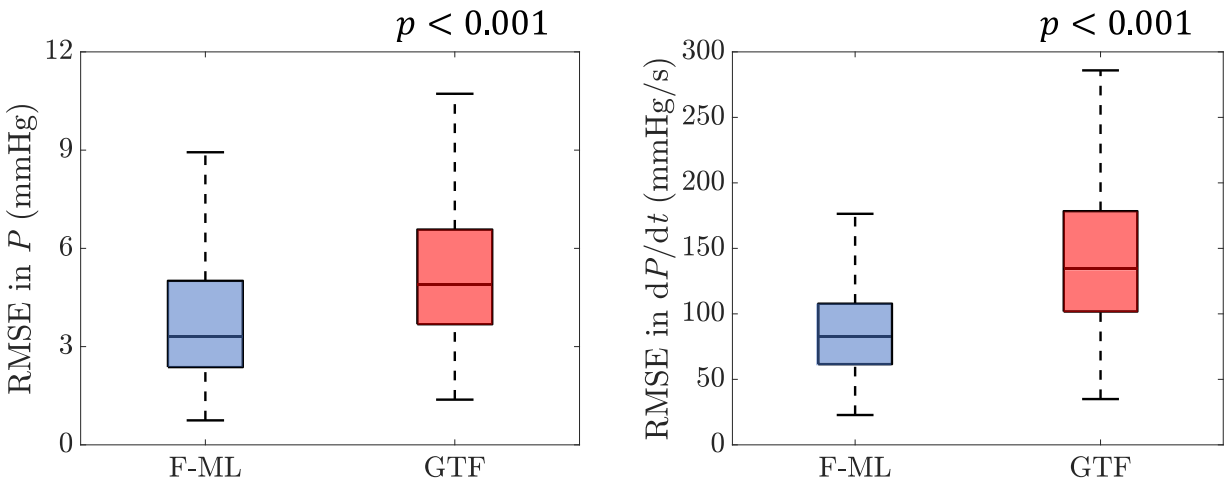

Fig. 6. Statistical analysis of the associated error between the transferred and measured pressure waveform and the first time derivative of the pressure waveform. The blue boxplots (left) present the results for the Fourier-based Machine Learning (F-ML) transfer function and the red boxplots (right) present the results for the generalized transfer function (GTF). The reported p-values are from the Kruskal-Wallis' test for comparison of the two methods. F-ML results are based on the support vector regressor. (For interpretation of the references to color in this figure legend, the reader is referred to the web version of this article.)

Table 4
Mean nRMSE between the transferred and measured central waveform in the blind test group ($N = 792$).

Machine learning model	Lasso	SVR	GBDT
Pressure waveform			
3 input Fourier modes	9.4	9.3	9.6
5 input Fourier modes	7.0	7.0	7.5
10 input Fourier modes	5.7	5.6	6.3
20 input Fourier modes	5.6	5.5	6.4
First derivative of the pressure waveform			
3 input Fourier modes	11.0	11.0	11.0
5 input Fourier modes	9.5	9.4	9.5
10 input Fourier modes	6.6	6.6	6.6
20 input Fourier modes	6.0	5.9	6.1
Second derivative of the pressure waveform			
3 input Fourier modes	13.5	13.5	13.5
5 input Fourier modes	13.1	13.1	13.1
10 input Fourier modes	10.5	10.5	10.5
20 input Fourier modes	9.1	9.0	9.3

Values are presented as percentage. SVR and GBDT stand for support vector regressor and gradient boosted decision tree. The reference nRMSE between the transferred pressure waveform using the GTF and the measured pressure waveform is 7.8 %, 9.3 %, and 19.4 % for the pressure waveform, first derivative of the pressure waveform and the second derivative of the pressure waveform.

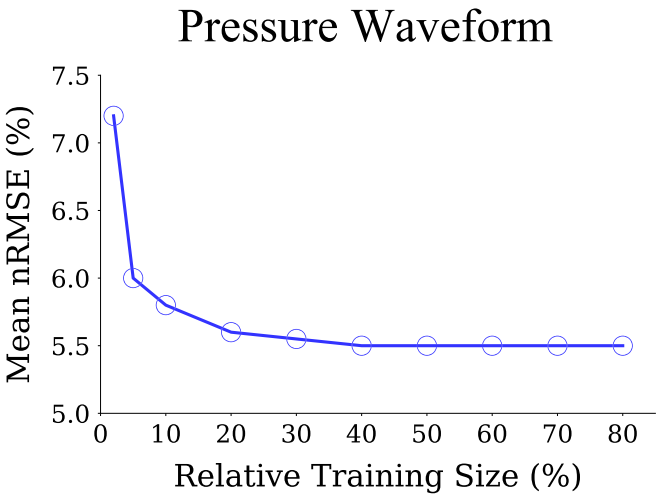

Fig. 7. Sensitivity of accuracy in terms of normalized root mean square (nRMSE) of the pressure waveform to the training size.

function is its ability in reconstructing the shape of the central pressure waveform from a peripheral measurement. Fig. 4 provides six sample test cases demonstrating the ability of the F-ML transfer function in reconstructing the central pressure waveform overlaid by the measured one. For reference, we demonstrated the transferred central pressure waveform using the GTF in this figure as well. To further examine the ability of the proposed method, we also computed the error associated with reconstructing the first and second derivative of the pressure waveform. These derivatives not only have mathematical value in terms of determining the shape of the pressure waveform, by itself they can provide valuable physiological information as it is shown in previous works [43,44]. In Fig. 5, we demonstrated the reconstructed first and second derivative of the pressure waveform using both transfer functions overlaid by the measured one. As it is shown by these two figures, the shape of the transferred waveform using F-ML is closer to the measured central waveform as it is compared with the transferred waveform using GTF. The first derivative and second derivative focus on highlighting the higher frequency components. Unlike in the GTF where each bin's averaged function is independent of others, our proposed F-ML approach considers the interaction of different modes when predicting each central output mode. This enables us to better capture nonlinear effects at higher frequencies. This is primarily why F-ML demonstrates a more significant performance improvement compared to GTF, especially for derivative waveforms. To quantitatively compare the accuracy of the proposed method with the GTF, we utilized nRMSE between the transferred waveform and the central measurement. Findings from Table 3 and Fig. 6 suggests that the accuracy of the reconstructed waveform using the F-ML transfer function is better than the GTF for the pressure waveform as well as its first and second derivatives. We have further assessed the accuracy of the F-ML transfer function using the form factor, which is a wave analysis metric providing information on waveform morphology. Form factor is defined as the ratio between the mean pulse pressure (MBP-DBP) and pulse pressure (SBP-DBP) [45,46]. The RMSE for form factor between our proposed model and measured one is 0.026 with mean value of 0.421 for the F-ML transferred pressure and 0.419 for the measured on. Notably, the RMSE for form factor between GTF and measured one is 0.043 (mean value of 0.401 for the GTF transferred pressure). These results further confirm

the better performance of the proposed F-ML approach compared to the conventional GTF.

We also found that choosing the number of Fourier modes to decompose the input pressure waveform to the machine has an impact on the correlation and the error of predicted pressure waveforms (Table 4). Depending on the chosen number of Fourier modes, some information about the pressure waveform may be missed as shown in Fig. S1. However, for the purpose of transferring the peripheral measurement to the central waveform, higher frequency features may not be necessarily required and hence it is essential to find the sufficient number Fourier modes for the transfer function. This is particularly important for reduced-order approaches for ML modeling. Results suggest that after 10 input Fourier modes, there is only a marginal improvement in the accuracy of the transfer function (Table 4). This can effectively expand the applicability of our proposed method for smaller datasets, which can be of particular interest in cardiovascular engineering [18]. Lastly, we examined the proposed F-ML transfer function's sensitivity to the relative training size of the utilized dataset in this study. The training size is modified from 90 % to 10 % of the total number of cases (Fig. 7). Results suggest that nRMSEs decreased gradually with increasing training size. The improvement in the accuracy however is negligible after the training size reaches 30 % of the dataset. Similar observation using other databases was reported by Bikia et al. [47]. Notably, our findings indicate that allocating 30 % of the complete dataset for training, equivalent to 792 instances, with an input size of 39 (representing 20 modes), results in an average of 20 instances per input. This ratio proves to be adequate for achieving accuracy with the proposed F-ML approach. This sensitivity analysis suggests that the employed training size for this study is sufficient. In addition, it suggests that given a sufficient input to the model, the method is generalizable to the larger population which is critical for the future use of this method.

4.1. Study limitations and future work

The major limitation in this study is that we do not have invasively measured aortic pressure waveforms for determining exact central pressure waveform. Future studies employing invasive clinical measurements can further expand the applicability of the proposed transfer function. However, our choice of using the carotid pressure waveform as a surrogate for aortic is well-established [36,37]. In addition, future studies can aim to include training data from multi-center datasets to further examine and expand the usage of the proposed Fourier-based machine learning transfer function.

5. Conclusion

In this study, we introduced a novel Fourier-based ML transfer function methodology aimed to reconstruct the central pressure waveform from peripheral measurement. We test this approach in a large heterogeneous sample of the Framingham Heart Study population. Our findings show that our novel method not only better captures the shape of the aortic pressure waveform compared to the generalized transfer function, but also accurately represents the major features of the central blood pressure including the systolic, diastolic, and mean blood pressure. Utilizing our approach, the estimation of central pressure waveforms in clinical cohorts can be significantly enhanced when the peripheral blood pressure wave is accessible. This may ultimately contribute to improving the clinical applicability of radial pressure monitoring in medical devices and wearable electronics.

Ethical statement

In terms of the ethical issues involved in enrolling patients in this study, all participants provided written informed consent and all protocols were approved by the Boston University Medical Center Institutional Review Board.

CRediT authorship contribution statement

Arian Aghilinejad: Conceptualization, Investigation, Methodology, Visualization, Writing – original draft, Writing – review & editing, Formal analysis. **Alessio Tamborini:** Formal analysis, Investigation, Methodology, Writing – review & editing. **Morteza Gharib:** Investigation, Resources, Supervision, Writing – review & editing.

Declaration of competing interest

The authors declare that they have no known competing financial interests or personal relationships that could have appeared to influence the work reported in this paper.

Acknowledgements

The Framingham Heart Study is conducted and supported by the National Heart, Lung, and Blood Institute (NHLBI) in collaboration with Boston University (Contract No. N01-HC-25195, HHSN268201500001I and 75N92019D00031). This manuscript was not prepared in collaboration with investigators of the Framingham Heart Study and does not necessarily reflect the opinions or views of the Framingham Heart Study, Boston University, or NHLBI.

Appendix A. Supplementary data

Supplementary data to this article can be found online at https://doi.org/10.1016/j.artmed.2024.102918.

References

[1] Wilkinson IB, Cockcroft JR, Webb DJ. Pulse wave analysis and arterial stiffness. J Cardiovasc Pharmacol 1998;32:S33–7.
[2] Nelson, M. R., Stepanek, J., Cevette, M., Covalciuc, M., Hurst, R. T., and Tajik, A. J., "Noninvasive measurement of central vascular pressures with arterial tonometry: clinical revival of the pulse pressure waveform?," Proc. Mayo Clinic Proceedings, Elsevier, pp. 460–472.
[3] Aghilinejad A, Alavi R, Rogers B, Amlani F, Pahlevan NM. Effects of vessel wall mechanics on non-invasive evaluation of cardiovascular intrinsic frequencies. J Biomech 2021;129:110852.
[4] Aghilinejad A, Amlani F, King KS, Pahlevan NM. Dynamic effects of aortic arch stiffening on pulsatile energy transmission to cerebral vasculature as a determinant of brain-heart coupling. Sci Rep 2020;10(1):1–12.
[5] Pahlevan NM, Tavallali P, Rinderknecht DG, Petrasek D, Matthews RV, Hou TY, et al. Intrinsic frequency for a systems approach to haemodynamic waveform analysis with clinical applications. Journal of The Royal Society Interface 2014;11 (98):20140617.
[6] Aghilinejad A, Wei H, Magee GA, Pahlevan NM. Model-based fluid-structure interaction approach for evaluation of thoracic endovascular aortic repair Endograft length in type B aortic dissection. Front Bioeng Biotechnol 2022;10.
[7] Aghilinejad A, Amlani F, Mazandarani SP, King KS, Pahlevan NM. Mechanistic insights on age-related changes in heart-aorta-brain hemodynamic coupling using a pulse wave model of the entire circulatory system. American Journal of Physiology-Heart and Circulatory Physiology 2023;325(5):H1193–209.
[8] Aghilinejad A, Rogers B, Geng H, Pahlevan NM. On the longitudinal wave pumping in fluid-filled compliant tubes. Phys Fluids 2023;35(9).
[9] O'rourke MF. Carotid artery tonometry: pros and cons. Am J Hypertens 2016;29 (3):296–8.
[10] Liu J, Sodini CG, Ou Y, Yan B, Zhang Y-T, Zhao N. Feasibility of fingertip oscillometric blood pressure measurement: model-based analysis and experimental validation. IEEE J Biomed Health Inform 2019;24(2):533–42.
[11] Liu J, Yan BP, Zhang Y-T, Ding X-R, Su P, Zhao N. Multi-wavelength photoplethysmography enabling continuous blood pressure measurement with compact wearable electronics. IEEE Transactions on Biomedical Engineering 2018; 66(6):1514–25.
[12] Rinderknecht D, De Balasy JM, Pahlevan NM. A wireless optical handheld device for carotid waveform measurement and its validation in a clinical study. Physiol Meas 2020;41(5):055008.
[13] Tamborini A, Gharib M. A pneumatic low-pass filter for high-fidelity cuff-based pulse waveform acquisition. Ann Biomed Eng 2023:1–12.
[14] Kang J, Aghilinejad A, Pahlevan NM. On the accuracy of displacement-based wave intensity analysis: effect of vessel wall viscoelasticity and nonlinearity. PloS One 2019;14(11):e0224390.
[15] Digiglio P, Li R, Wang W, Pan T. Microflotronic arterial tonometry for continuous wearable non-invasive hemodynamic monitoring. Ann Biomed Eng 2014;42: 2278–88.

[16] Liu J, Pahlevan NM. The underlying mechanism of intersite discrepancies in ejection time measurements from arterial waveforms and its validation in the Framingham Heart Study. American Journal of Physiology-Heart and Circulatory Physiology 2021;321(1):H135–48.
[17] Karamanoglu M, O'Rourke MF, Avolio AP, Kelly RP. An analysis of the relationship between central aortic and peripheral upper limb pressure waves in man. Eur Heart J 1993;14(2):160–7.
[18] Magbool A, Bahloul MA, Ballal T, Al-Naffouri TY, Laleg-Kirati T-M. Aortic blood pressure estimation: a hybrid machine-learning and cross-relation approach. Biomedical Signal Processing and Control 2021;68:102762.
[19] Liu W, Du S, Pang N, Zhang L, Sun G, Xiao H, et al. Central aortic blood pressure waveform estimation based on temporal convolutional network. IEEE J Biomed Health Inform 2023;27(7):3622–32.
[20] Zhang Y, Asada HH. Blind system identification of noncoprime multichannel systems and its application to noninvasive cardiovascular monitoring. J Dyn Sys, Meas, Control 2004;126(4):834–47.
[21] Stergiopulos N, Westerhof BE, Westerhof N. Physical basis of pressure transfer from periphery to aorta: a model-based study. American Journal of Physiology-Heart and Circulatory Physiology 1998;274(4):H1386–92.
[22] Gao M, Rose WC, Fetics B, Kass DA, Chen C-H, Mukkamala R. A simple adaptive transfer function for deriving the central blood pressure waveform from a radial blood pressure waveform. Sci Rep 2016;6(1):33230.
[23] Mariscal-Harana J, Charlton PH, Vennin S, Aramburu J, Florkow MC, van Engelen A, et al. Estimating central blood pressure from aortic flow: development and assessment of algorithms. American Journal of Physiology-Heart and Circulatory Physiology 2021;320(2):H494–510.
[24] Patel AM, Li JK, Finegan B, McMurtry MS. Aortic pressure estimation using blind identification approach on single input multiple output nonlinear wiener systems. IEEE Transactions on Biomedical Engineering 2017;65(6):1193–200.
[25] Chen S, Ji Z, Wu H, Xu Y. A non-invasive continuous blood pressure estimation approach based on machine learning. Sensors 2019;19(11):2585.
[26] Viunytskyi, O., Shulgin, V., Sharonov, V., and Totsky, A., "Non-invasive cuff-less measurement of blood pressure based on machine learning," Proc. 2020 IEEE 15th International Conference on Advanced Trends in Radioelectronics, Telecommunications and Computer Engineering (TCSET), IEEE, pp. 203–206.
[27] Tavallali P, Razavi M, Pahlevan NM. Artificial intelligence estimation of carotid-femoral pulse wave velocity using carotid waveform. Sci Rep 2018;8(1):1–12.
[28] Bikia V, Pagoulatou S, Trachet B, Soulis D, Protogerou AD, Papaioannou TG, et al. Noninvasive cardiac output and central systolic pressure from cuff-pressure and pulse wave velocity. IEEE J Biomed Health Inform 2019;24(7):1968–81.
[29] Aghilinejad A, Wei H, Bilgi C, Paredes A, DiBartolomeo A, Magee GA, et al. Framework development for patient-specific compliant aortic dissection phantom model fabrication: magnetic resonance imaging validation and deep-learning segmentation. J Biomech Eng 2023;145(9):091010.
[30] Jin W, Chowienczyk P, Alastruey J. Estimating pulse wave velocity from the radial pressure wave using machine learning algorithms. PloS One 2021;16(6):e0245026.
[31] Aghilinejad A, Wei H, Pahlevan NM. Non-invasive pressure-only aortic wave intensity evaluation using hybrid Fourier decomposition-machine learning approach. IEEE Transactions on Biomedical Engineering 2023;70(2):2139–48.
[32] Du S, Liu W, Yao Y, Sun G, He Y, Alastruey J, et al. Reconstruction of the aortic pressure waveform using a two-level adaptive transfer function strategy. Measurement 2022;204:112111.
[33] Cooper LL, Rong J, Benjamin EJ, Larson MG, Levy D, Vita JA, et al. Components of hemodynamic load and cardiovascular events: the Framingham Heart Study. Circulation 2015;131(4):354–61.
[34] Mitchell GF, Hwang S-J, Vasan RS, Larson MG, Pencina MJ, Hamburg NM, et al. Arterial stiffness and cardiovascular events: the Framingham Heart Study. Circulation 2010;121(4):505–11.
[35] Cooper LL, Rong J, Pahlevan NM, Rinderknecht DG, Benjamin EJ, Hamburg NM, et al. Intrinsic frequencies of carotid pressure waveforms predict heart failure events: the Framingham Heart Study. Hypertension 2021;77(2):338–46.
[36] Kelly R, Fitchett D. Noninvasive determination of aortic input impedance and external left ventricular power output: a validation and repeatability study of a new technique. J Am Coll Cardiol 1992;20(4):952–63.
[37] Kelly R, Hayward C, Avolio A, O'rourke M. Noninvasive determination of age-related changes in the human arterial pulse. Circulation 1989;80(6):1652–9.
[38] Bikia V, Papaioannou TG, Pagoulatou S, Rovas G, Oikonomou E, Siasos G, et al. Noninvasive estimation of aortic hemodynamics and cardiac contractility using machine learning. Sci Rep 2020;10(1):1–17.
[39] Hughes AD, Park C, Ramakrishnan A, Mayet J, Chaturvedi N, Parker KH. Feasibility of estimation of aortic wave intensity using non-invasive pressure recordings in the absence of flow velocity in man. Front Physiol 2020;11:550.
[40] Hughes AD, Parker KH. The modified arterial reservoir: an update with consideration of asymptotic pressure (P∞) and zero-flow pressure (Pzf). Proceedings of the Institution of Mechanical Engineers, Part H: Journal of Engineering in Medicine 2020;234(11):1288–99.
[41] Michail M, Hughes AD, Comella A, Cameron JN, Gooley RP, McCormick LM, et al. Acute effects of transcatheter aortic valve replacement on central aortic hemodynamics in patients with severe aortic stenosis. Hypertension 2020;75(6):1557–64.
[42] Aghilinejad A, Amlani F, Liu J, Pahlevan NM. Accuracy and applicability of non-invasive evaluation of aortic wave intensity using only pressure waveforms in humans. Physiol Meas 2021;42(10):105003.
[43] Abel FL. Maximal negative dP/dt as an indicator of end of systole. American Journal of Physiology-Heart and Circulatory Physiology 1981;240(4):H676–9.
[44] Simek J, Wichterle D, Melenovsky V, Malik J, Svacina S, Widimsky J. Second derivative of the finger arterial pressure waveform: an insight into dynamics of the peripheral arterial pressure pulse. Physiol Res 2005;54(5):505.
[45] Salvi P. Pulse waves. In: How vascular hemodynamics affects blood pressure; 2012.
[46] Alavi R, Aghilinejad A, Wei H, Niroumandi S, Wieman S, Pahlevan NM. A coupled atrioventricular-aortic setup for in-vitro hemodynamic study of the systemic circulation: design, fabrication, and physiological relevancy. PloS One 2022;17(11):e0267765.
[47] Bikia V, Rovas G, Pagoulatou S, Stergiopulos N. Determination of aortic characteristic impedance and total arterial compliance from regional pulse wave velocities using machine learning: an in-silico study. Front Bioeng Biotechnol 2021;9:649866.